

Joint modeling of the probability distribution and power spectrum of the Ly α forest : comparison with observations at $z = 3$

Vincent Desjacques¹ and Adi Nusser^{1,2}

¹ The Physics Department and the Asher Space Research Institute, Technion, Haifa 32000, Israel

² The Institute for Advanced Study, School of Natural Sciences, Einstein Drive, Princeton, NJ 08540

Email : dvince@physics.technion.ac.il, adi@physics.technion.ac.il

arXiv:astro-ph/0410618v1 26 Oct 2004

23 May 2019

ABSTRACT

We present results of joint modeling of the probability distribution function (PDF) and the one-dimensional power spectrum (PS) of the Ly α forest flux decrement. The sensitivity of these statistical measures to the shape and amplitude of the linear matter power spectrum is investigated using N-body simulations of two variants of the Λ CDM cosmology. In the first model, the linear power spectrum has a scale-invariant spectral index $n_s = 1$, whereas in the second, it has a negative running index (RSI), $dn/dlnk < 0$. We generate mock catalogs of QSO spectra, and compare their statistical properties to those of the observations at $z = 3$. We perform a joint fit of the power spectrum and the PDF. A scale-invariant model with $\sigma_8 = 0.9$ matches well the data if the mean IGM temperature is $T \lesssim 1.5 \times 10^4$ K. For higher temperature, it tends to overestimate the flux power spectrum over scales $k \lesssim 0.01$ s km $^{-1}$. The discrepancy is less severe when the PS alone is fitted. However, models matching the PS alone do not yield a good fit to the PDF. A joint analysis of the flux PS and PDF tightens the constraints on the model parameters and reduces systematic biases. The RSI model is consistent with the observed PDF and PS only if the temperature is $T \gtrsim 2 \times 10^4$ K. The best fit models reproduce the slope and normalisation of the column density distribution, irrespective of the shape and amplitude of the linear power spectrum. They are also consistent with the observed line-width distribution given the large uncertainties. Our joint analysis yields $\sigma_8 = 0.8 \pm 0.1$ for a temperature $1 \lesssim T \lesssim 2 \times 10^4$ K and a reasonable reionization history.

Key words: cosmology: theory – gravitation – dark matter – baryons – intergalactic medium

1 INTRODUCTION

Absorption features in the Ly α forest provide direct information on the large scale distribution of neutral hydrogen in the highly ionized intergalactic medium (Bahcall & Salpeter 1965; Gunn & Peterson 1965; see e.g. Rauch 1998 for a review). The Ly α forest is believed to trace the warm photoionized, fluctuating intergalactic medium (IGM) which smoothly traces the distribution of the dark matter. This is sustained by hydrodynamical simulations which have succeeded in reproducing the observed statistics of the absorption lines and transmitted flux (e.g. McGill 1990; Bi 1993; Cen *et al.* 1994; Zhang, Anninos & Norman 1995; Petitjean, Mücke & Kates 1995; Hernquist *et al.* 1996; Katz *et al.* 1996; Miralda-Escudé *et al.* 1996; Hui, Gnedin & Zhang

1997; Theuns *et al.* 1998). The Ly α forest, therefore, serves as a probe the physical state of the IGM, and the underlying matter distribution over a wide range of scales and redshifts (e.g. Croft *et al.* 1998; Nusser & Haehnelt 2000; Schaye *et al.* 2000). Several method have been proposed for recovering the shape and amplitude of the primordial power spectrum, $\Delta_L^2(k)$ (e.g. Croft *et al.* 1998, 2002; McDonald *et al.* 2000; McDonald 2003). The current methods rely on an inversion of the one-dimensional flux power spectrum $\Delta_F^2(k)$, and the calibration of the nonlinear relation between the matter and flux power spectra by means of detailed numerical simulations (e.g. Croft *et al.* 2002; McDonald 2003). These methods are fundamentally limited by continuum fitting errors, metal contamination and nonlinear corrections (e.g. Hui *et al.* 2001; Zaldarriaga, Scoccimarro & Hui 2003;

see also Gnedin & Hamilton 2002). Furthermore, one has to marginalize over the ‘nuisance’ parameters in order to place constraints on the spectral index n_s and the normalisation amplitude σ_8 . Underestimating the mean flux level $\langle F \rangle$, for example, can strongly bias the results as it was shown by Seljak, McDonald & Makarov (2003), and Viel, Haehnelt & Springel (2004). Recent analyses of the Ly α forest favour a simple scale-invariant model with σ_8 in the range 0.85–0.95 (McDonald *et al.* 2004b; Viel, Haehnelt & Springel 2004; Viel, Weller & Haehnelt 2004; Seljak *et al.* 2004). Nevertheless, the systematic errors in inverting the one dimensional flux power spectrum into the three dimensional linear mass power spectrum could be larger than expected. It is, therefore, prudent to examine how other statistical measures of the forest constrain the cosmological model.

Here we follow a different strategy in analyzing the Ly α flux decrement. First, we use three statistical measures of the forest in assessing the validity of cosmological models. These measures are the one dimensional flux power spectrum, $\Delta_F^2(k)$, the flux probability distribution function (PDF), $P(F)$, and the neutral hydrogen column density distribution $f(N_{\text{HI}})$. Second, we adopt the “forward approach” in which the validity of a cosmological model is assessed by comparing the observed statistical measures with those directly derived from N-body simulations of the cosmological model under consideration (see e.g. Zaldarriaga, Hui & Tegmark 2001). This approach has the advantage of not requiring any inversion procedure to obtain the linear mass power spectrum.

Combining several statistical measures could significantly affect the constraints on the shape and amplitude of the primordial power spectrum as inferred from $\Delta_F^2(k)$ alone. In this paper, we will attempt to match simultaneously the three statistics mentioned above. In principle, higher order statistics such as the bispectrum should also be considered since they provide independent information on the cosmology (e.g. Mandelbaum *et al.* 2003). However, the Ly α bispectrum as computed from high-resolution QSO spectra is still too noisy to provide significant constraints on the cosmological model (e.g. Viel *et al.* 2004a). To explore a parameter space as large as possible, we will implement a simple semi-analytical model which reproduce many properties of the Ly α absorbers (e.g. Bi, Börner & Chu 1992; Reisenegger & Miralda-Escudé 1995; Bi & Davidsen 1997; Gnedin & Hui 1998). We generate a wide sample of mock catalogs and constrain the model parameters by comparing their statistical properties to observational data.

The paper is organized as follows. In Section §2 we briefly review the observations we use in this analysis. In §3, we detail the method we use to compute synthetic spectra from pure dark matter (DM) simulations. The comparison between simulation and observations is done in §4. We discuss our results in §5.

2 OBSERVATIONAL DATA

In this paper we will compare the simulations to the flux power spectrum and PDF measured by McDonald *et al.*

Table 1. The main parameters of the Λ CDM simulations considered in the present paper. The normalisation of the RSI simulations follows from the results of Spergel *et al.* (2003).

	Ω_m	Ω_Λ	h	σ_8	$m/[10^8 h^{-1} M_\odot]$
S1 and S2	0.30	0.70	0.70	0.90	0.76
R1 and R2	0.31	0.69	0.71	0.84	0.81

(2000) (hereafter M00), which were obtained from a sample of eight high-resolution QSO spectra. Regarding the flux power spectrum, we consider the data points in the range $0.005 < k < 0.04 \text{ s km}^{-1}$. The lower limit $k = 0.005 \text{ s km}^{-1}$ is set by the size of our simulations (cf. Section §3.1). Note that it is below the scale $1/k \sim 300 \text{ km s}^{-1}$ where continuum fitting errors are expected to become important (e.g. Hui *et al.* 2001). The upper limit $k = 0.05 \text{ s km}^{-1}$ is chosen because of concern about metal contamination on smaller scales (e.g. M00; Kim *et al.* 2004). The observed flux PDF is very sensitive to continuum fitting, especially in the high transmissivity tail. We therefore exclude the data points with $F \geq 0.8$ from the analysis to avoid dealing with continuum fitting error. In addition, we discard also the measurement at $F = 0$ since it is strongly affected by noise (e.g. Rauch *et al.* 1997). Finally, we emphasize that we work with the power spectrum of the transmitted flux F , which differs from that of the flux density contrast, $\delta_F \equiv (F/\langle F \rangle - 1)$, by a multiplicative factor $\langle F \rangle^2$.

3 MODELLING THE Ly α FOREST

In this Section, we will first describe the DM simulations in detail. We will then briefly review the basic ingredients relevant to create realistic Ly α spectra from simulations of DM only.

3.1 The N-body simulations

We run DM simulations of a Λ CDM cosmology with the N-body code GADGET (Springel, Yoshida & White 2001). Pure DM simulations are more suitable to our purposes since they allow us to explore a larger parameter space than full hydrodynamical simulations. To reproduce the Ly α forest as seen in QSO spectra and, at the same time, resolve typical absorption systems, a large volume together with a high resolution are requested (e.g. Theuns *et al.* 1998; Bryan *et al.* 1999). For this reason, each simulation evolves 256^3 particles of mass $m \sim 10^8 M_\odot/h$ in a periodic box of size $25 h^{-1} \text{ Mpc}$. Since cosmic variance error on, e.g., the optical depth normalisation (at constant mean flux) can be relatively large when estimated from such a small volume (e.g. Croft *et al.* 2002), we have performed two random realisations for each of the model we consider in the present paper. In the simulations which we denote S1 and S2, the initial power spectrum is scale-invariant, $n_s = 1$ (Eisenstein & Hu 1999). In the simulations R1 and R2, the initial power spectrum is that of the RSI model (e.g. Spergel 2003). The present-day

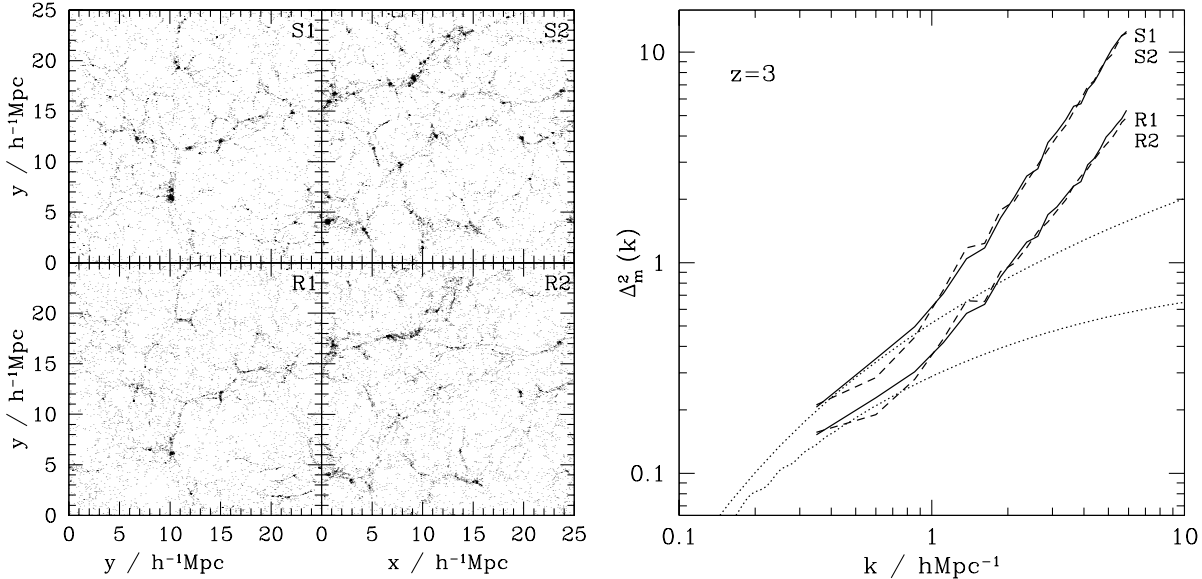


Figure 1. *Left panel* : The particle distribution in a slice of thickness $\Delta h = 0.05 h^{-1}\text{Mpc}$ through the various ΛCDM simulations at $z = 3$: the scale-invariant realisations S1 and S2 (top panels), and the RSI realisations R1 and R2 (bottom panels). *Right panel* : The corresponding 3D power spectra $\Delta_m^2(k)$ computed at $z = 3$ from the DM particle distribution. The dashed curves show $\Delta_m^2(k)$ for the S2 and R2 simulations. The dotted curves show the linear power spectrum used to seed the fluctuations.

normalisation amplitude of these simulations, $\sigma_8 = 0.84$, is slightly lower than that of S1 and S2, for which $\sigma_8 = 0.9$. The initial particle positions were computed using a parallel code kindly provided by Volker Springel. The cosmological parameters are summarized in Table 1. In the left panel of Fig. 1, we show a slice of thickness $\Delta h = 0.05 h^{-1}\text{Mpc}$ extracted from the four simulations at redshift $z = 3$. Note that the simulations S1 and R1 (S2 and R2) have the same random seed.

To quantify how the various simulations differ, we plot in Fig. 1 the dimensionless 3D matter power spectrum $\Delta_m^2(k)$ at $z = 3$ for all the simulations. It was obtained by CIC sampling the DM particles onto a 512^3 grid and taking the Fourier transform by means of a FFT routine. As we can see, R1 and R2 exhibit much less power than S1 and S2. On scale $k \sim 3 h\text{Mpc}^{-1}$, which corresponds to the pivot point in the flux power spectrum (cf. Figure 4), $\Delta_m^2(k)$ in the scale-invariant simulations is about twice as large as it is in the RSI simulations. Cosmic variance becomes important on scale $k \lesssim 1 h\text{Mpc}^{-1}$, where the matter power spectrum computed from the S1 (R1) realisation is larger than that of S2 (R2) by about 10-20%. We also show the linear power spectra which we use to seed fluctuations in the initial DM distribution as dotted curves. The largest scale of the simulations, $k \lesssim 1 h\text{Mpc}^{-1}$, are still in the linear regime at $z = 3$. On scale $k \lesssim 0.1 h\text{Mpc}^{-1}$, the power spectrum of the RSI model is very close to that of the $n_s = 1$ model.

3.2 Generating mock catalogs of QSO spectra

3.2.1 The low density IGM

Semi-analytical models of the Ly α forest exploit the tight relationship between the gas and the underlying DM distribution (e.g. Bi 1993; Bi & Davidsen 1997; Petitjean *et al.* 1995; Gnedin & Hui 1998; Croft *et al.* 1998). In this approach, the gas temperature T_g , and the neutral hydrogen density n_{HI} are computed using tight powerlaw relations obtained from full hydrodynamical simulations (e.g. Katz *et al.* 1996, Hui & Gnedin 1997, Theuns *et al.* 1998),

$$T_g = \hat{T}_g (1 + \delta_g)^{\gamma-1} \quad \text{and} \quad n_{\text{HI}} = \hat{n}_{\text{HI}} (1 + \delta_g)^\alpha , \quad (1)$$

where the adiabatic index γ is in the range $1 - 1.62$, and $\alpha = 2 - 0.7(\gamma - 1)$. \hat{T}_g and \hat{n}_{HI} are the temperature and neutral hydrogen density at mean gas density respectively. These scaling relations hold for moderate gas overdensities, i.e. $\delta_g \lesssim 50$. For higher overdensities however, we have to account for line cooling. To this extent, we follow Desjacques *et al.* (2004) and take the gas temperature to be $T_g = 10^4 \text{ K}$ for $\delta\rho/\rho > 50$. This cutoff ensures that the Doppler parameter $b(\mathbf{x})$ is always $b(\mathbf{x}) = 13 \text{ km s}^{-1}$ in the high density regions of the simulation.

When radiative cooling is inefficient, it is reasonable to assume that the gas density and velocity fields, δ_g and \mathbf{v}_g , are smoothed versions of their DM counterparts, δ_m and \mathbf{v}_m . We obtain the gas density distribution by sampling the DM particles onto a 512^3 grid, and smoothing the resulting density field with a Gaussian filter $W = \exp(-k^2/2k_F^2)$ of characteristic length $1/k_F$. This choice is motivated by the fact that a Gaussian filter gives a good fit to the gas fluctuations over a wide range of wavenumbers. Furthermore,

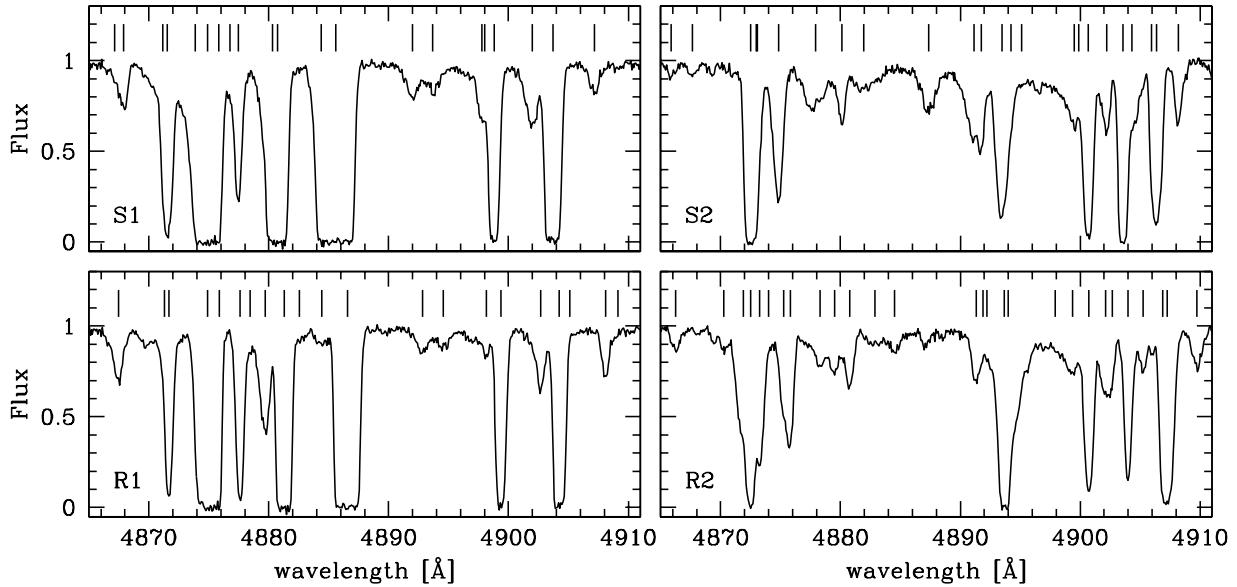


Figure 2. Synthetic spectra extracted from each of the simulations at $z = 3$. The vertical bars above the spectra show the position of the lines with fitted column densities N_{HI} exceeding $10^{12.5} \text{ cm}^2$. The comoving length of each spectrum is $L = 25 h^{-1} \text{ Mpc}$, which corresponds to a redshift interval $\Delta z \sim 0.04$ at $z = 3$.

we expect k_F to depend on the physical state of the IGM. However, since the relation between k_F and \hat{T}_g depends noticeably on the reionization history of the Universe (Gnedin & Hui 1998), it is more convenient to treat k_F as a free parameter (see e.g. Zaldarriaga, Hui & Tegmark 2001). We discuss gas smoothing in more detail in Appendix §A.

3.2.2 The synthetic spectra

Once we have smoothed the DM density and velocity fields on the filtering scale $1/k_F$, the flux distribution depends only on the mean flux $\langle F \rangle$, the adiabatic index γ and the mean IGM temperature \hat{T}_4 . For any value taken by the four-dimensional parameter vector $\mathbf{p} = (k_F, \langle F \rangle, \gamma, \hat{T}_4)$, we generate mock catalogs as follows. For each of the simulations, we randomly select 10^4 lines of sight (LOS) of comoving length $L = 25 h^{-1} \text{ Mpc}$. Next, the optical depth τ and the transmitted flux $F = \exp(-\tau)$ are computed along each LOS in 512 pixels of width $\Delta v \simeq 6 \text{ km s}^{-1}$ according to the Gunn-Peterson approximation (Gunn & Peterson 1965). Note that the spectral resolution is somewhat smaller than that of the M00 data, where it is $\Delta v = 6.6 \text{ km s}^{-1}$. Finally, the value of \hat{n}_{HI} is adjusted such that the mean flux $\langle F \rangle$ of the whole sample matches the desired value (e.g. Rauch *et al.* 1997). To account for the noise in the observations, we add a uniform Gaussian deviate of dispersion $\sigma = 0.02$ per interval of width $\Delta\pi = 2.5 \text{ km s}^{-1}$.

In Fig. 2, we plot four synthetic spectra selected from each of our simulations. The spectra were extracted from mock samples which, for a given simulation, give an acceptable fit to the observed statistics of the Ly α forest (cf. Section §4). In particular, we have respectively $\hat{T}_4 = 1.5$ and 2

for the scale-invariant (top panels) and RSI models (bottom panels). Ticks above the spectra mark the Ly α absorption lines which were identified with the spectral fitting program VPFIT (Carswell *et al.* 2003). The lines are distinguished by their column density N_{HI} (in cm^{-2}) and their width or Doppler parameter b (in km s^{-1}). This fitting technique assumes that the fundamental shape of the lines is a Voigt profile, which is a good approximation for column densities $N_{\text{HI}} \lesssim 10^{17} \text{ cm}^{-2}$ relevant to the Ly α forest. Absorption systems with column density $N_{\text{HI}} \leq 10^{12.5} \text{ cm}^2$ are quite uncertain and are not shown on the figure (e.g. Bi & Davidsen 1997). The spectra extracted from R1 and R2 feature somewhat more lines than those extracted from S1 and S2. The reason is the larger clustering of the scale-invariant models. As a result, blending of absorbers to form one strong line occurs more often, and cause the number of lines identified with VPFIT to be lower than that in the R1 and R2 models. Note that, in practice, associated metal lines can help fixing the number of subcomponents. We will discuss the properties of the simulated column density distribution in Section §4.4.

4 COMPARISON WITH OBSERVATIONS

In this Section, we compare the statistical properties of our mock catalogs to that of the observations. We perform a χ^2 statistics for the observed flux power spectrum and PDF. We also compare the simulated line column density and line-width distributions to observational data for several models.

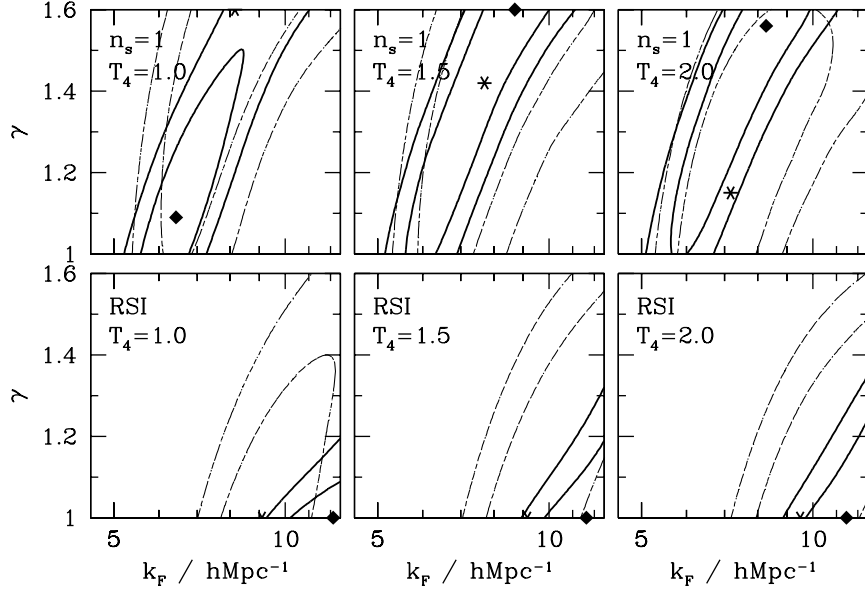


Figure 3. Constraints in the plane $k_F\gamma$ for a scale-invariant cosmology with $\sigma_8 = 0.9$ (top panels), and a RSI cosmology (bottom panels). The contours show the 1 and 2σ confidence levels (assuming a Gaussian likelihood). The mean IGM temperature is $\hat{T}_4 = 1$ (left panels), 1.5 (middle panels) and 2 (right panels). The constraint arising from measurements of the flux PS solely is shown as dashed contours, while that arising from the combination of the flux PS and PDF is shown as solid contours. The stars and diamonds mark the best fit models obtained from the PS and PS+PDF data respectively.

4.1 The parameter grid

For each value of our parameter vector $\mathbf{p} = (k_F, \langle F \rangle, \gamma, \hat{T}_4)$, we generate mock catalogs of ten thousand lines of sight. We let the parameters assume the following values,

$$\begin{aligned} k_F &= 4.55, 5, 5.56, 6.25, 7.14, 8.33, 10, 12.5 \\ \gamma &= 1, 1.1, 1.2, 1.3, 1.4, 1.5, 1.6 \\ \hat{T}_4 &= 0.5, 1, 1.5, 2, 2.5 \\ \langle F \rangle &= 0.65, 0.66, 0.67, 0.68, 0.69, 0.7, 0.71, 0.72, 0.73 \end{aligned}$$

The values of k_F (in unit of $h\text{Mpc}^{-1}$) were chosen such that $1/k_F$ uniformly spans the range $0.08\text{--}0.22 h^{-1}\text{Mpc}$. Our discrete grid thus contains $8 \times 9 \times 7 \times 5 = 2520$ models. For each mock catalog, we then calculate the flux power spectrum and the flux PDF, and average over the S1 and S2 (resp. R1 and R2) realisations. We then determine the goodness of fit of any model in the grid by computing a χ^2 statistics from the difference between the simulated PS, PDF and the observational data. We account for measurements of the mean flux $\langle F \rangle$ by adding a term $(\langle F \rangle - \bar{F})^2/\sigma_{\bar{F}}^2$ to the chi-squared, where $\bar{F} = 0.684$ and $\sigma_{\bar{F}} = 0.023$ are the observed mean flux and error bar at $z = 3$ (see Table 1 of McDonald *et al.* 2000). The problem of finding the best fit models is equivalent of finding the maximum of some hypersurface. Since the true maximum does not generally lies exactly at a grid point, it is desirable to interpolate over the different parameters. To this extent, we take advantage of the smooth dependence of the flux PS and PDF on the parameter vector, and use cubic spline interpolation. This method is known to work substantially better than a simple multi-linear interpolation (e.g. Tegmark & Zaldarriaga 2000). To marginalize over a subset of the parameters, we fix their values to that of the

best fit model of the subspace, which we obtained from the spline interpolation. To check the accuracy of the interpolation, we computed the flux PS and PDF from the simulations for several randomly selected models which do not lie at a grid point. We found that the flux PS and PDF of the spline-interpolated models differ from that of the 'true' models by $\lesssim 0.5\%$ only in the range of scales considered in our analysis.

Correlation among the data points is a major source of uncertainty. In the case of the flux power spectrum, we can assume in a good approximation that the data points are uncorrelated. In the case of the PDF however, the data points are strongly correlated. As a result, the χ^2 distribution as computed from the diagonal elements of the error matrix solely might differ noticeably from that computed from the full error matrix (see e.g. M00; Gnedin & Hamilton 2002). The χ^2 should therefore be computed from the full covariance matrix. However, the covariance matrix of the observed PDF (available at <http://www.astronomy.ohio-state.edu/~jordy/lya>) features spurious large, negative off-diagonal elements which spoil the computation of the chi-squared. We decided therefore to restrict ourselves to the diagonal elements.

Since the spectral fitting program is relatively slow, we have not included the line distribution in the χ^2 statistics. We will compute the line statistics only for models which best fit the PS and PDF (cf. Section §4.4).

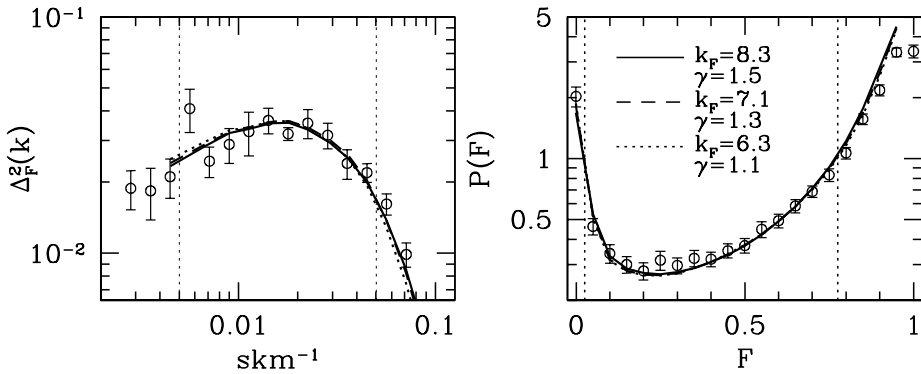


Figure 4. Three scale-invariant models which give an acceptable fit to the observed flux PS and PDF. The mean IGM temperature is $\hat{T}_4 = 1.5$. The reduced chi-squared are $\chi^2 = 23.5, 23.2$ and 22.8 (for 23 degrees of freedom) for $\gamma = 1.5, 1.3$ and 1.1 respectively. Only the data points which lie between the two vertical lines were used to compute the χ^2 statistics.

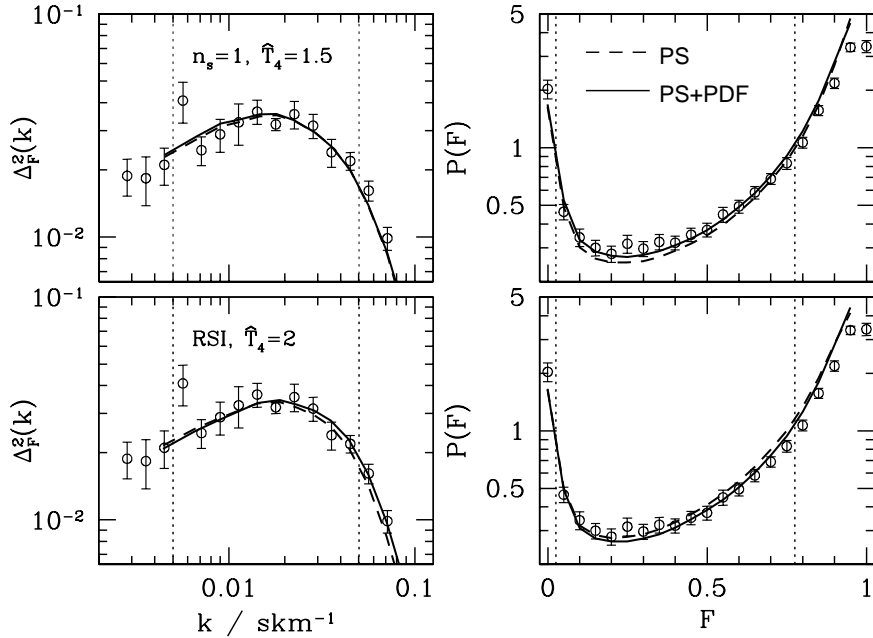


Figure 5. A comparison between models which best fit the PS data alone (dashed curves), and models which best fit the PS+PDF data (solid curves). They are shown for a scale-invariant cosmology with $\hat{T}_4 = 1.5$ (top panels), and for the RSI cosmology with $\hat{T}_4 = 2$ (bottom panels).

4.2 The flux power spectrum and probability distribution

4.2.1 Constraint in the k_F - γ plane

Fig. 3 shows the constraints in the plane k_F - γ for the scale-invariant cosmology with normalisation $\sigma_8 = 0.9$ (top panels) and for the RSI cosmology (bottom panels). The mean IGM temperature is $\hat{T}_4 = 1$ (left panels), 1.5 (middle panels) and 2 (right panels). The contours show the 68.3% and 95.5% confidence levels (assuming a Gaussian distribution for the likelihood) obtained from the flux power spectrum

alone (dashed curves), and from a combination of the flux PS and PDF data (solid curves). There is obviously a degeneracy between the filtering length $1/k_F$ and the adiabatic index γ . For illustration, we plot in Fig. 4 the PS and PDF of three scale-invariant models which fit the PS and PDF data at the 1σ level. The IGM temperature is $\hat{T}_4 = 1.5$. The models are plotted together with the measurements of M00, shown as empty symbols. As we can see, though these models differ in the value of k_F and γ , they all yield very similar power spectra and PDFs. To understand the origin of this degeneracy, note that increasing γ generally reduces the width of the weak lines, $\tau \lesssim 1$, whereas it enhances the

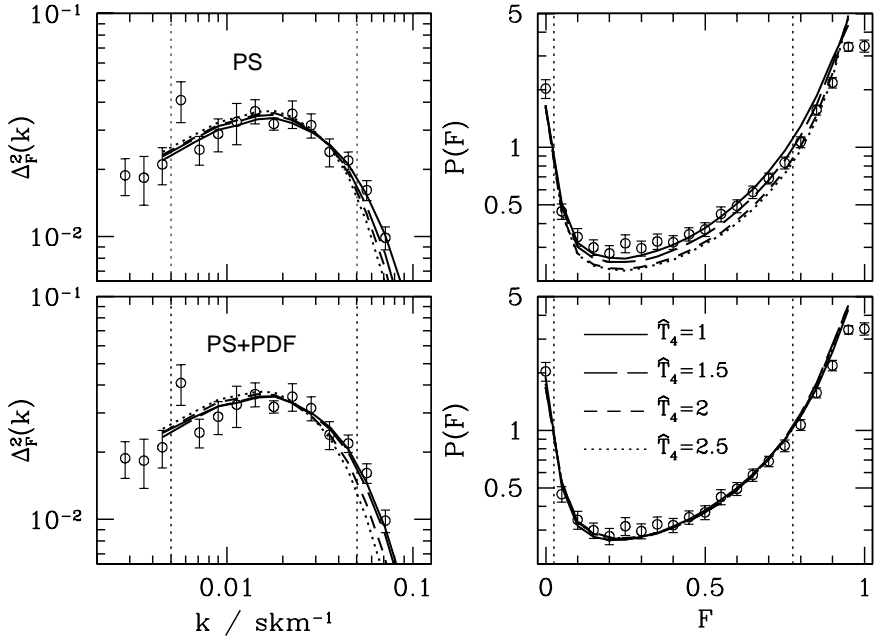


Figure 6. Scale-invariant models which fit best the PS data solely (top panels), and the PS+PDF data (bottom panels) as a function of the mean IGM temperature. The temperature is $\hat{T}_4 = 1$ (solid), 1.5 (long-dashed), 2 (short-dashed) and 2.5 (dotted) curves.

width of the strong lines, $\tau \gtrsim 1$. This follows from the fact that the low column density Ly α forest arises in gas of low overdensity (see e.g. Schaye 2001). Consequently, increasing γ (at constant mean flux) decreases $\Delta_F^2(k)$ on small scale, and thereby mimics the effect of a smaller k_F . In the PDF, increasing γ increases the fraction of transmissivity pixels in the range $F \gtrsim 0.5$ presumably because, at constant mean flux, the lower optical depth normalisation and the reduction in the width of the weak lines conspire to increase the fraction of high transmissivity pixels. As a result, the combination of the PS and PDF cannot break this degeneracy since both statistics exhibit a similar dependence on k_F and γ . In reality however, one would expect the filtering length to depend on \hat{T}_g and γ (see Appendix §A). Therefore, additional assumptions on the reionization history of the Universe could break this degeneracy. In this respect, the observed line-width distribution suggests that, around $z = 3$, there is a sharp increase in \hat{T}_g together with a decrease in γ (Schaye *et al.* 2000; Ricotti, Gnedin & Shull 2000; see however McDonald *et al.* 2001). However, the data are too noisy to constrain \hat{T}_4 and γ significantly.

4.2.2 The best fit models

In Fig. 3, the stars and squares symbols mark the models which best fit the PS and PS+PDF data, respectively. These models are compared in Fig. 5 to the M00 data. The temperature of the scale-invariant models was chosen to be $\hat{T}_4 = 1.5$, while the RSI models have $\hat{T}_4 = 2$. This choice is motivated by the fact that, in a scale-invariant cosmology with $\sigma_8 = 0.9$, models with $\hat{T}_4 \lesssim 1.5$ fit the data best whereas, in a RSI cosmology, the best fit are obtained for $\hat{T}_4 \gtrsim 2$

(cf. Table 2). The RSI models match the observed $\Delta_F^2(k)$ somewhat better than the scale-invariant models. However, they tend to overestimate the PDF in the range $F \gtrsim 0.6$, which roughly traces regions of gas overdensity $\delta_g \lesssim 0$. This follows from the relative lack of small-scale power, which translates into larger values of the PDF in the high transmissivity tail. Consequently, matching the flux PDF in a RSI cosmology requires a low filtering length. Indeed, though the RSI models which best fit the PS data alone have $k_F \lesssim 10 \text{ hMpc}^{-1}$, those which best fit the PS+PDF data have $k_F \gtrsim 11 \text{ hMpc}^{-1}$, close to the largest value assumed by k_F in our parameter grid. Since the Nyquist frequency of the grid is $k_{Ny} \sim 10.2 \text{ hMpc}^{-1}$, these models are certainly affected by numerical resolution. However, numerical resolution also contributes to the smoothing (e.g. Zaldarriaga, Hui & Tegmark 2001), and $k_F = 11 \text{ hMpc}^{-1}$ is merely a lower limit. Note that we have $k_F \sim 6 - 9 \text{ hMpc}^{-1}$ for the best scale-invariants models, a filtering scale which is robust to resolution issues.

Fig. 5 also shows clearly that models which match best the PS data alone do not yield a good fit of the PDF. It is therefore important to combine the two statistics in order to ensure that both the PS and PDF are correctly reproduced. The constraints inferred from measurements of $\Delta_F^2(k)$ alone might thus be significantly biased. To quantify this effect, we plot in Fig. 6 the flux power spectrum and PDF of scale-invariant models for several values of \hat{T}_g . Models which fit best the PS and the PS+PDF data are shown in the top and bottom panels, respectively. When the PS data alone are fitted, the agreement between the observed and simulated flux PDF worsens with increasing temperature. For $\hat{T}_4 \gtrsim 2$, the disagreement is very severe. A comparison between the top and bottom left panels reveals that including the PDF in the

χ^2 statistics increases the amplitude of flux power spectrum by an amount of $\sim 10\%$ on scale $k \lesssim 0.01 \text{ s km}^{-1}$. Increasing the temperature produces a similar but weaker effect : the large-scale amplitude of $\Delta_F^2(k)$ decreases by about 5% when the temperature increases from $\hat{T}_4 = 1$ to 2. Note that the strength of this effect is consistent with findings from hydrodynamical simulations (e.g. Viel, Haehnelt & Springel 2004). Combining the PS and PDF data could therefore reduce the best fit value of σ_8 by about 10%. We also expect a degeneracy between the normalisation amplitude and the mean IGM temperature. As a result, decreasing σ_8 should help us matching the data with a larger IGM temperature. We will discuss this point in more detail in Section §4.3.

The photoionisation rate Γ_{-12} of the neutral hydrogen (in unit of 10^{-12} s^{-1}) can be estimated from the optical depth normalisation τ_0 , which can be written as

$$\tau_0 = 2.31 \mathcal{A}(z) \hat{T}_4^{-0.7} \left(\frac{1+z}{4} \right)^6, \quad (2)$$

where $\mathcal{A}(z) = (\Omega_b h^2 / 0.02)^2 H_{100}(z)^{-1} \Gamma_{-12}(z)^{-1}$. Here, Ω_b is the baryon content and $H(z)$ the Hubble constant in unit of $100 \text{ km s}^{-1} \text{ Mpc}^{-1}$ (e.g. Rauch *et al.* 1997; McDonald *et al.* 2000). To calculate Γ_{-12} , we assume $\Omega_b h^2 = 0.02$, in agreement with the constraint derived from CMB and deuterium abundance measurements (e.g. Spergel *et al.* 2003; Burles & Tytler 1998). For the models of Fig. 5 which best fit the PS+PDF data, the optical depth normalisation is $\tau_0 \sim 0.9$ (scale-invariant) and ~ 0.8 (RSI). The inferred photoionisation rate for both best fit models is $\Gamma_{-12} \sim 0.6$, a value consistent with other estimates (e.g. Rauch *et al.* 1997; McDonald & Miralda-Escudé 2001). This result confirms that our simulations fully resolve the Ly α forest.

4.3 Sensitivity to the normalisation amplitude

As we discussed before, a scale-invariant cosmology of normalisation $\sigma_8 = 0.9$ matches best the data when \hat{T}_4 is low. However, we could improve the agreement with the data in the range $\hat{T}_4 \gtrsim 1.5$ by decreasing the rms density fluctuations. To assess the sensitivity of the statistics to the normalisation amplitude σ_8 , we take advantage of the self-similarity of gravitational clustering in EdS cosmology (a good approximation at redshift $z \gtrsim 2$). As a result, a snapshot at redshift different from $z = 3$, once rescaled, can mimic a cosmology with a different σ_8 . Since the fluctuation amplitude of the RSI model is tightly constrained by the CMB and Ly α forest data (e.g. Bennett *et al.* 2003; Spergel *et al.* 2003), we will vary σ_8 in the scale-invariant cosmology only. We consider snapshots separated by a redshift interval $\Delta z = 0.2$ in the range $z = 2 - 4$. These snapshots thus mimic scale-invariant cosmologies of rms density fluctuation $0.7 \lesssim \sigma_8 \lesssim 1.1$.

4.3.1 Correlation between σ_8 and \hat{T}_g

In Fig. 7, we compare the PS (left panel) and the PDF (right panel) of several best fit models with different normalisation

Table 2. Parameter values of scale-invariant and RSI models which best fit the PS+PDF data, for a mean IGM temperature $\hat{T}_4 = 1, 1.5, 2$ and 2.5 . The filtering k_F is in unit of $h\text{Mpc}^{-1}$. The last column gives the chi-squared for 23 degrees of freedom (25 data points minus two free parameters). Note that, since we spline interpolate over the parameters, the best fit values do not necessarily lie at a grid point.

model	\hat{T}_4	$\langle F \rangle$	k_F	γ	χ^2
$n_s = 1, \sigma_8 = 0.72$	1	0.69	7.2	1	21.4
	1.5	0.70	11.1	1.6	18.9
	2	0.70	10.2	1.53	21.0
	2.5	0.70	8.8	1.37	24.9
$n_s = 1, \sigma_8 = 0.82$	1	0.69	6.6	1	20.9
	1.5	0.69	9.7	1.6	21.4
	2	0.70	9.1	1.55	25.1
	2.5	0.70	8.1	1.42	30.4
$n_s = 1, \sigma_8 = 0.9$	1	0.69	6.5	1.16	21.3
	1.5	0.69	8.8	1.6	23.7
	2	0.69	8.2	1.55	28.4
	2.5	0.69	7.7	1.45	34.9
$n_s = 1, \sigma_8 = 1$	1	0.68	6.9	1.29	21.3
	1.5	0.69	8.0	1.57	25.4
	2	0.69	7.9	1.56	32.0
	2.5	0.69	7.0	1.42	39.9
RSI	1	0.7	12.1	1	31.3
	1.5	0.7	11.6	1	25.7
	2	0.7	11.5	1	22.2
	2.5	0.7	12.5	1.07	20.6

amplitude : $\sigma_8 = 0.72$ (solid), 0.82 (long-dashed), 0.9 (short dashed) and 1 (dashed-dotted curves). We also show the best fit RSI model as a dotted curve. The mean IGM temperature was chosen to be $\hat{T}_4 = 1.5$. For sake of completeness however, we list in Table 2 the parameters values of best fit models for a mean IGM temperature in the range $1 \leq \hat{T}_g \leq 2.5$. A comparison between the RSI and the scale-invariant $\sigma_8 = 0.82$ models, which have very similar normalisation amplitudes, demonstrates that $\Delta_F^2(k)$ on scale $k \lesssim 0.01 \text{ s km}^{-1}$ is very sensitive to the small-scale behaviour of the matter power spectrum. Indeed, the difference in the flux power spectrum of these two models mainly results from including the PDF in the chi-squared statistics. This shows that combining several statistics of the Ly α forest can help constraining the shape of the linear power spectrum.

The scale-invariant models reasonably fit the flux power spectrum and PDF. However, the large-scale amplitude of $\Delta_F^2(k)$ increases with σ_8 , and causes the models with $\sigma_8 \gtrsim 0.9$ to overestimate the data on scale $k \lesssim 0.01 \text{ s km}^{-1}$. To assess how significant is this effect, we need an estimate for the cosmic variance error in the flux PS. To this purpose, we ran two additional simulations (S3 and S4) of a scale-invariant cosmology with normalisation $\sigma_8 = 0.9$ and computed the flux PS and PDF for the best fit models of Fig. 7. Next, from the sample of simulations $S1 \rightarrow S4$, we computed the flux PS and PDF for the six possible combinations of two simulations. The cosmic variance error was then the 1σ scatter around the mean. We also accounted for the finite number of mock spectra in the cosmic variance. In Fig. 7, the cosmic variance error is shown for the model with $\sigma_8 = 0.9$ as er-

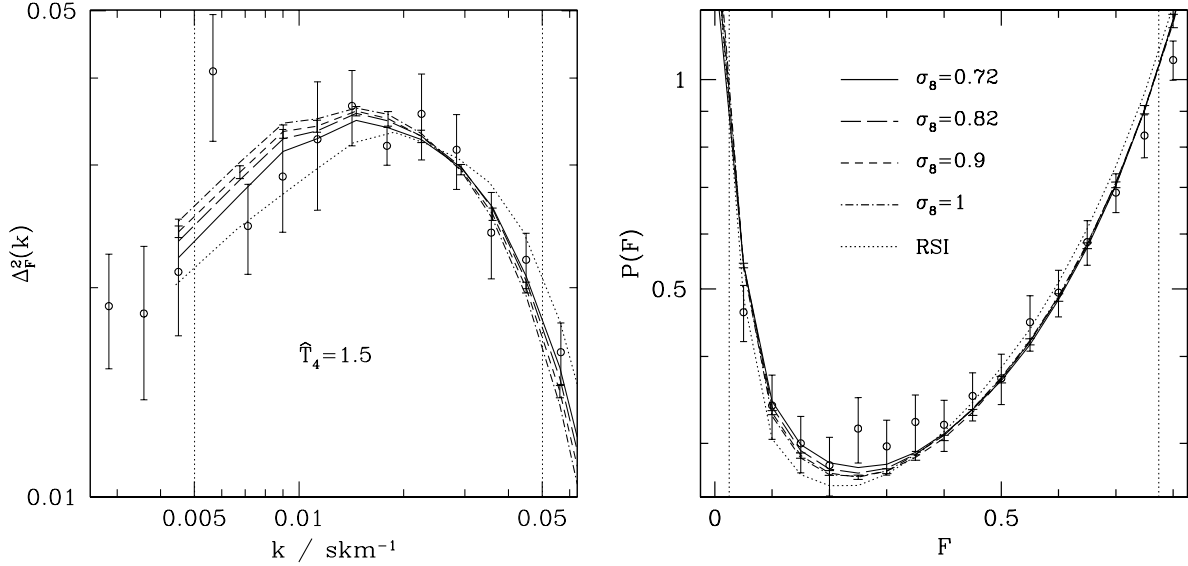


Figure 7. A comparison between the flux PS (left panel) and PDF (right panel) of scale-invariant models with rms density fluctuation $\sigma_8 = 0.72$ (solid), 0.82 (long-dashed), 0.9 (short dashed) and 1 (dashed-dotted curve). The RSI model is shown as dotted curves. All the models have a temperature $\hat{T}_4 = 1.5$. The errorbars attached to the model with σ_8 show our estimate of the cosmic variance error (cf. text).

rorbars. The errors do not change much among the various models. They are small, about $\lesssim 3\%$ and $\lesssim 2\%$ in the flux PS and PDF respectively. However, since our simulations lack of large-scale power, our calculation probably underestimates the cosmic variance error. Nevertheless, even if they were twice as large, the flux PS of models with $\sigma_8 \gtrsim 0.9$ would still lie above the data points on scale $k \lesssim 0.01 \text{ skm}^{-1}$. This effect is thus real. Moreover, it increases with the temperature. As a result, there is a degeneracy between \hat{T}_g and σ_8 (at constant mean flux $\langle F \rangle$). A model with larger σ_8 requires a lower temperature to match the flux PS. Note, however, that the measurement errors are large in that range of wavenumber. As a result, although the models with $\sigma_8 \gtrsim 0.9$ shown in Fig. 7 predict a $\Delta_F^2(k)$ which, by eye, overestimates the observations in that range of wavenumber, they are still consistent with the data in a χ^2 sense at least (The worst chi-squared, $\chi^2 = 25.4$ for 23 degrees of freedom, is obtained for $\sigma_8 = 1$, and corresponds to a fit probability $\sim 30\%$).

To illustrate the correlation which exists between the mean IGM temperature and the normalisation amplitude, we plot in Fig. 8 the difference $\Delta\chi^2 = \chi^2 - \chi^2_{\min}$ as a function of the normalisation amplitude, after marginalizing over the mean flux level. The mean IGM temperature is $\hat{T}_g = 1$ (left panel), 1.5 (middle panel) and 2 (right panel). The adiabatic index has a fixed value $\gamma = 1.3$, consistent with that inferred from observations at $z \sim 3$ (e.g. Schaye *et al.* 2000; Ricotti, Gnedin & Shull 2000; McDonald *et al.* 2001). The filtering is $k_F = 8.3$ (solid curve), 7.1 (long-dashed) and 6.3 hMpc^{-1} (short-dashed). The reason for selecting particular values of γ and k_F follows from the fact that it is difficult to marginalize over these parameters since they are degenerated. The large measurement errors worsen the situation. However, we can take advantage of the degeneracy (i.e. the subspace $k_F\gamma$ has one effective degree of freedom)

by fixing γ to some value and varying k_F without restricting the analysis. Note also that the wiggles which appear in $\Delta\chi^2$ are caused by numerical instabilities in the marginalization step. Fig. 8 shows that, at a given filtering k_F , decreasing the temperature increases the best fit value of σ_8 . Moreover, at fixed temperature, decreasing the filtering k_F also increases the best fit σ_8 . For e.g. $\hat{T}_4 = 1.5$, we find $\sigma_8 \approx 0.71, 0.83$ and 0.96 for $k_F = 8.3, 7.1$ and 6.3 hMpc^{-1} . In other words, one needs to increase the clustering amplitude in order to compensate for the larger smoothing. As a result, it would therefore be possible to match the data with a normalisation $\sigma_8 \gtrsim 1$ if both the filtering and the IGM temperature are very low, $k_F \approx 6 \text{ hMpc}^{-1}$ and $\hat{T}_4 \approx 1$. A model where $k_F = 6.3 \text{ hMpc}^{-1}$ and $\hat{T}_4 = 1$ has a best fit value $\sigma_8 = 1.06$, and fits the data with an acceptable chi-squared $\chi^2 = 22.4$ for 24 degrees of freedom.

4.3.2 A temperature-dependent filtering

A model with $\sigma_8 \gtrsim 1$ can match the data if both \hat{T}_g and k_F are very low. However, we would expect k_F to be relatively larger for a temperature $\hat{T}_4 \sim 1$. To make further progress, we we will assume that the filtering k_F is a function of the mean IGM temperature \hat{T}_g . We discuss in more detail the dependence of k_F on the IGM temperature and the reionization history of the Universe in Appendix §A. To summary, we expect the filtering scale decrease with increasing temperature as $k_F \propto \hat{T}_4^{-1/2}$. Furthermore, the filtering scale $k_F(\hat{T}_4 = 1) \equiv k_F(1)$ at $z = 3$ should be larger than $\sim 8 \text{ hMpc}^{-1}$ for reasonable reionization scenarios. In order to illustrate the effect of such a relation on the flux PS and PDF, we show in Fig. 9 $\Delta\chi^2$ as a function of σ_8 after marginalizing over the mean flux. The tem-

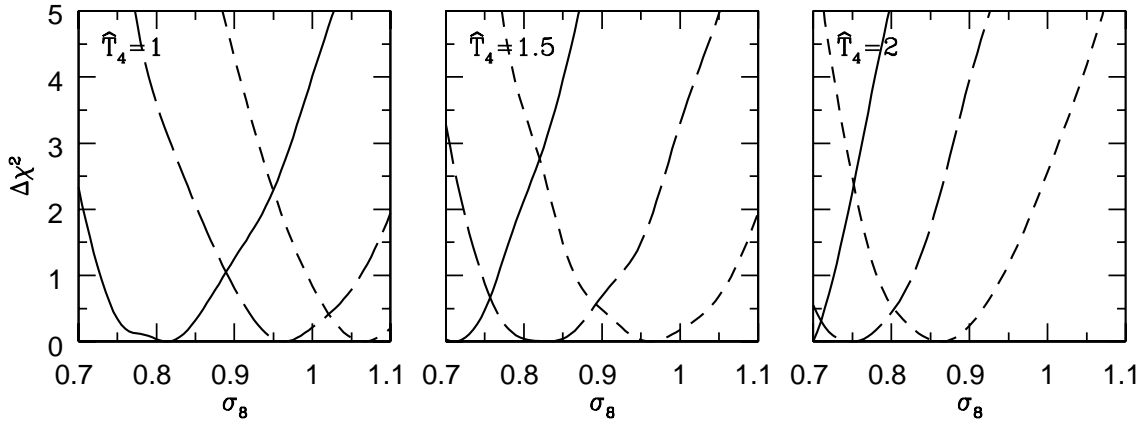


Figure 8. Constraint on σ_8 from a fit to the observed flux PS and PDF. The curves show $\Delta\chi^2 = \chi^2 - \chi^2_{\min}$ for a mean IGM temperature $\hat{T}_4 = 1$ (left panel), 1.5 (middle panel) and 2 (right panel) after marginalizing over the mean transmitted flux $\langle F \rangle$. The filtering is $k_F = 8.3$ (solid curve), 7.1 (long-dashed) and 6.3 $hMpc^{-1}$ (short-dashed). The adiabatic index has a fixed value $\gamma = 1.3$.

perature is $\hat{T}_4 = 1$ (solid curves), 1.5 (long-dashed) and 2 (short-dashed). We assume $k_F = 10\hat{T}_4^{-1/2}$ (curves with triangles) and $8\hat{T}_4^{-1/2} hMpc^{-1}$ (curves with squares), which would correspond to $\eta \approx 1.4$ and ≈ 1.1 respectively for $\gamma = 1.3$. These relatively low values should nonetheless not be taken too seriously given the uncertainties in the relation between baryons and dark matter. However, we believe that $k_F(1) = 8 hMpc^{-1}$ is a reasonable lower limit on the filtering k_F at $z = 3$ (cf. Appendix A). The best fit models are listed in Table 3 for various temperature, assuming a fixed $\gamma = 1.3$. The corresponding flux power spectrum and PDF are shown in Fig. 10. The best fit value of σ_8 now increases with the temperature as a result of temperature dependent filtering. Furthermore, since reionization is more efficient in a Universe of larger rms density fluctuations, i.e. $k_F(1)$ is smaller, we would expect the best fit value of σ_8 to increase with decreasing $k_F(1)$. Fig. 9 shows that this is indeed the case. We have $\sigma_8 \sim 0.9$ and $\sigma_8 \sim 0.75$ for $k_F(1) = 8$ and $10 hMpc^{-1}$ respectively. The models with $k_F(1) = 10 hMpc^{-1}$ are consistent with the data, whereas those with $k_F(1) = 8 hMpc^{-1}$ tend to overestimate $\Delta_F^2(k)$ on scale $k \lesssim 0.01 s km^{-1}$ when the temperature is large, $\hat{T}_4 \gtrsim 1.5$. Indeed, given that $k_F(1) = 8 hMpc^{-1}$ is a reliable upper limit on the filtering scale $1/k_F$, the normalisation amplitude should be less than ~ 0.9 . It is difficult to derive a lower limit on the filtering scale since we expect the corresponding k_F to be larger than $k_{Ny} \sim 10 hMpc^{-1}$. However, if we assume $k_F(1) > 10 hMpc^{-1}$, the best fit values of σ_8 we obtain from spline interpolation are $\sigma_8 \gtrsim 0.65$, even for a very high temperature $\hat{T}_4 \gtrsim 2$. Therefore, we expect $0.7 \lesssim \sigma_8 \lesssim 0.9$ for a reasonable choice of reionization history, and a temperature $1 \lesssim \hat{T}_4 \lesssim 2$.

4.4 The observed line statistics

To assess whether the best fit models reproduce the observed line statistics, we compute the column density and line width distributions, and compare our results to observational data.

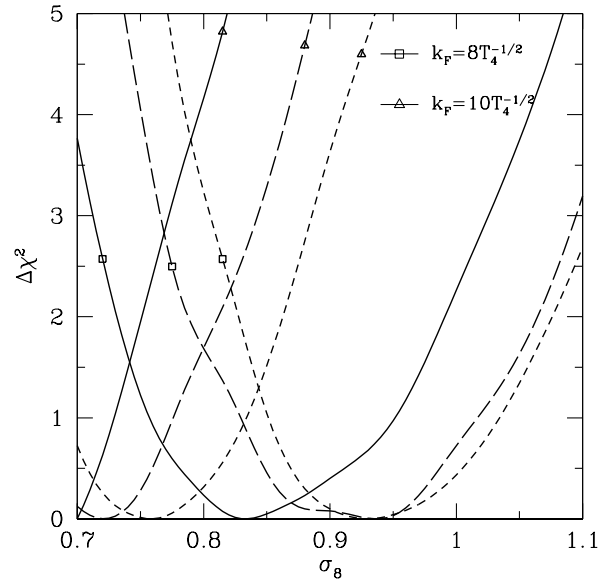


Figure 9. $\Delta\chi^2$ for a mean IGM temperature $\hat{T}_4 = 1$ (solid curves), 1.5 (long-dashed) and 2 (short-dashed) after marginalizing over the mean flux level. We assume that the filtering depends on the IGM temperature according to $k_F \propto \hat{T}_4^{-1/2}$, with $k_F = 8\hat{T}_4^{-1/2}$ (curves with squares) and $10\hat{T}_4^{-1/2} hMpc^{-1}$ (curves with triangles). The adiabatic index has a fixed value $\gamma = 1.3$.

4.4.1 The column density distribution

The differential line density distribution $f(N_{HI})$ is defined as the number of lines per unit column density and per unit absorption distance, which at redshift $z \sim 3$ is approximated by $X(z) = 2/3 [(1+z)^{3/2} - 1]$. In the left panel of Fig. 11 we plot the column density distribution for several models which give a good fit of the PS and PDF data ($\chi^2/\nu \lesssim 1$). $f(N_{HI})$ was calculated from a sample of 40 LOS. The simulated curves are compared to the data of Hu *et al.* (1995) and Petitjean *et al.* (1993), which are shown as filled circles

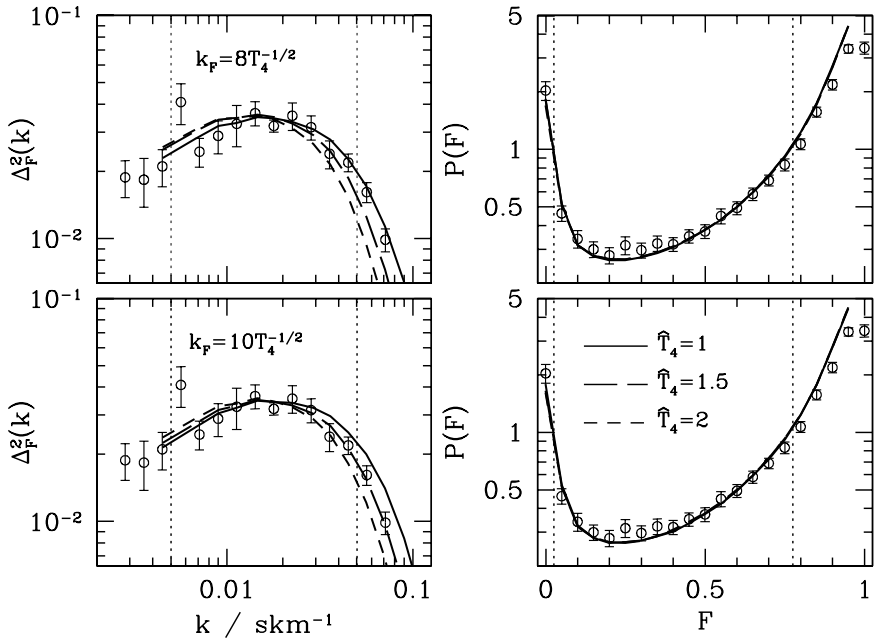


Figure 10. The flux power spectrum and PDF of the best fit models of Fig. 9. The adiabatic index has a fixed value $\gamma = 1.3$, whereas the IGM temperature is $\hat{T}_4 = 1$ (solid curves), 1.5 (long-dashed) and 2 (short-dashed). The corresponding values of σ_8 are $\sigma_8 = 0.84$, 0.94, 0.93 (top panels) and $\sigma_8 = 0.67$, 0.72, 0.76 (bottom panels).

and squares respectively. The mean redshift of both samples is $z = 2.8$. We consider two scale-invariant, $\sigma_8 = 0.9$ models with different values of k_F and γ : $(k_F, \gamma) = (8.3, 1.5)$ (solid curve) and $(6.3, 1.1)$ (solid-dotted curve). In addition, we show $f(N_{\text{HI}})$ for a cold ($\hat{T}_4 = 1.5$) and a hot ($\hat{T}_4 = 2.5$) scale-invariant model of normalisation $\sigma_8 = 0.72$ as long- and short-dashed curves respectively. The RSI model is shown as a dotted curve. Absorption lines with column density $10^{12.5} \leq N_{\text{HI}} \leq 10^{15.5} \text{ cm}^{-2}$ contribute most to the Ly α forest. In that range, the simulated column density distributions agree very well with the data. In particular, the slope and the normalisation of the simulated distributions coincides with that of the observations. They tends also to flatten in the range $N_{\text{HI}} \gtrsim 10^{14} \text{ cm}^{-2}$. Such a deviation from a single power law is also found in the observations (e.g. Petitjean *et al.* 1993; Kim *et al.* 1997). Fig. 11 demonstrates that, though the flux PS and PDF of the best fit models is rather sensitive to the normalisation amplitude and the relative amount of small-scale power (cf. Section §4.3), the column density distribution barely changes among the various models. If most of the lines identified by VPFIT have a column density $N_{\text{HI}} \lesssim 10^{15.5} \text{ cm}^{-2}$ ($\sim 10^3$ for a sample of 40 LOS), absorption systems with column density exceeding $N_{\text{HI}} \gtrsim 10^{15.5}$ are rare (~ 25). It is however crucial to reproduce them since they can contribute up to 50% of the flux power spectrum on scale $k \lesssim 0.01 \text{ skm}^{-1}$ (e.g. Viel *et al.* 2004b). Although the column density distribution suffers from the shot noise associated to these rare events, the left panel of Fig. 11 shows clearly that our simulations reproduce, at least quantitatively, these strong absorption systems.

4.4.2 The line-width distribution

The line-width distribution, $f(b)$, which is the fraction of line with a given width, is shown in the right panel of Fig. 11 for the models plotted in the left panel. $f(b)$ is computed from absorption systems with column density $10^{12.5} - 10^{14.5} \text{ cm}^{-2}$. The solid histogram is the data of Hu *et al.* (1995). The observed line-width distribution clearly exhibits a peak in the range $b \sim 20 - 40 \text{ km s}^{-1}$. In this respect, Fig. 11 shows that in the simulations, the peak is more pronounced for a model with larger value of γ at constant σ_8 . Furthermore, the scale-invariant model with lower normalisation ($\sigma_8 = 0.72$) and the RSI model account somewhat better for the amplitude of the observed peak, $f(b) \sim 0.04$. However, given the large measurement errors, it is very difficult to use $f(b)$ in order to constrain the parameter of the model. We conclude that the line statistics of the best fit models agree well with the observations, irrespective of the shape and amplitude of the matter power spectrum.

4.5 Systematic errors

Various sources of error affect our analysis, among them systematics in the data and in the modelling of the Ly α forest. Regarding the data, note that the M00 measurements, obtained from a sample of 8 QSO only, are quite noisy. In the flux power spectrum for example, the data point at $k = 0.00566 \text{ skm}^{-1}$ lies well above the others. One might worry that our results are strongly affected on this single data point. However, the corresponding error, $\sim 20\%$, is larger than that of the other data points. For the best fit

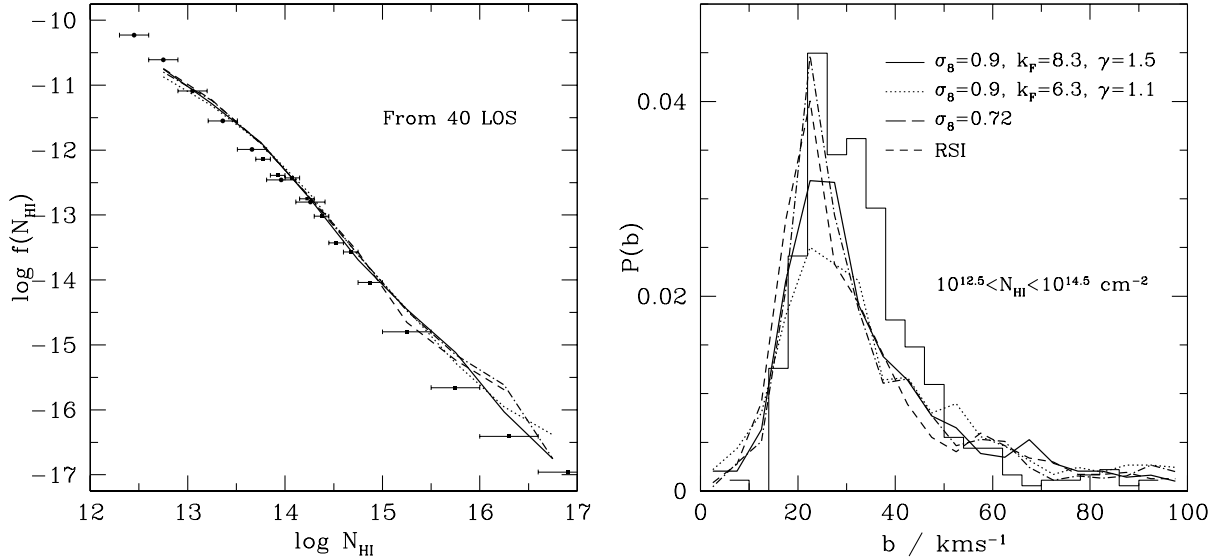


Figure 11. *Left panel* : The differential column density distribution $f(N_{\text{HI}})$ of various models which fit the PS and PDF data best : two scale-invariant models of normalisation $\sigma_8 = 0.9$ which have $(k_F, \gamma) = (8.3, 1.5)$ (solid curve) and $(6.3, 1.1)$ (dotted-dashed curve), a scale-invariant model with $\sigma_8 = 0.72$ (long-dashed curve), and a RSI model (short-dashed curve). The scale-invariant models have a temperature $\hat{T}_4 = 1.5$, while the RSI model has $\hat{T}_g = 2$. The filled circles and squares are the data of Hu *et al.* (1995) and Petitjean *et al.* (1993) respectively. *Right panel* : the corresponding line-width distribution $f(b)$. Only the lines with column density $N_{\text{HI}} = 10^{12.5} - 10^{14.5} \text{ cm}^{-2}$ were taken into account. The simulated distributions are compared to the data of Hu *et al.* (1995) shown as an histogram.

model with normalisation $\sigma_8 = 0.9$ shown in Fig. 7, the contribution of this data point to the chi-squared of the PS measurements ($\chi^2 = 10.4$) is $\Delta\chi^2 = 2.86$, smaller than that of the data point at $k = 0.00713 \text{ s km}^{-1}$, for which $\Delta\chi^2 = 4.45$. Indeed, we found that removing this data point from the chi-squared does not affect the results noticeably.

Continuum fitting errors are likely to affect the flux probability distribution. Modelling these errors is difficult because the scales of interest are of the order of the box size L of the simulations. However, M00 were able to demonstrate that, if the inclusion of continuum fitting errors can account for most of the discrepancy between the simulated and observed PDF in the range $F \gtrsim 0.8$, it should not affect much the PDF for $F \lesssim 0.8$. We thus believe that the PDF in the range $F \lesssim 0.8$ is robust to these errors. Continuum fitting errors might also affect the inferred column densities N_{HI} . However, the deviation from a single power-law in the regime $N_{\text{HI}} \lesssim 10^{14} \text{ cm}^{-2}$ is most probably caused by line blending, and by the nonlinear evolution of the structures associated to the absorption systems (e.g. Kim *et al.* 2002). Finally, they should play a minor role in the flux power spectrum since the scales probed by our simulations are relatively small, $k \gtrsim 0.003 \text{ s km}^{-1}$ (e.g. Kim *et al.* 2004).

Our semi-analytical model of the Ly α forest is well suited for our purposes since it allows us to explore a much larger parameter space than full hydrodynamical simulations. However, it does not account for shock heating, for the scatter in the temperature-density relation of the low IGM, nor for the dependence of the filtering length on the local gas density and temperature. Hydrodynamical simulations predict that shock heating should have driven a significant fraction of the baryons into the warm-hot phase of the in-

tergalactic medium (WHIM) at low redshift. At the present epoch, this fraction might be as large as 40% (e.g. Cen & Ostriker 1999; Davé *et al.* 2001; see also Nath & Silk 2001). At redshift $z \sim 3$ however, this fraction falls below 10%. Moreover, numerical simulations also show that most of the WHIM baryons at $z \sim 3$ resides in overdensities $\delta_g \gtrsim 10$ (Davé *et al.* 2001). Hence, shock heating should not affect the Ly α forest much at $z \sim 3$. Inhomogeneities in the UV background might also affect the flux power spectrum. However, this effect should not be too important on the scales ($k \gtrsim 0.05 \text{ s km}^{-1}$) and redshifts ($z = 3$) of interest (e.g. Croft 2004; McDonald *et al.* 2004c). Consequently, we expect the absence of scatter in the temperature-density relation and the assumption of uniform smoothing to contribute most to the modelling error. These approximations might translate into large systematic errors in the inferred values of σ_8 (e.g. Viel, Haehnelt & Springel 2004).

5 DISCUSSION

We have used N-body simulations of variants of the Λ CDM models to generate synthetic spectra of the Ly α forest. We have simulated the standard Λ CDM cosmology with scale-invariant spectral index models, as well as a running spectral index (RSI) model (Spergel *et al.* 2003). The one-dimensional flux power spectrum (PS) and flux probability distribution function (PDF) have been computed from mock catalogs, and compared to the observational data in order to constrain the cosmological models and the key physical parameters that dictate the properties of the Ly α forest. In addition to the PS and PDF comparison, we have also com-

Table 3. Parameter values of the models which best fit the flux PS and PDF, assuming a temperature-dependent smoothing. The filtering scale $k_F(1)$ (cf. text) is given in unit of $h\text{Mpc}^{-1}$. The adiabatic index has a fixed value $\gamma = 1.3$, whereas the mean IGM temperature is $\hat{T}_4 = 1, 1.5$ and 2 . The last columns gives the best fit values of $\langle F \rangle$, σ_8 and the corresponding χ^2 (for 24 degrees of freedom).

filtering	γ	\hat{T}_4	$\langle F \rangle$	σ_8	χ^2
$k_F(1) = 10$	1.3	1	0.68	0.67	24.9
		1.5	0.69	0.72	21.7
		2	0.69	0.76	25.3
$k_F(1) = 8$	1.3	1	0.68	0.84	22.4
		1.5	0.68	0.94	25.4
		2	0.68	0.93	38.7

puted the neutral hydrogen column density distribution and the line width distribution. These last two statistics have only been used as a consistency check to the models which best fitted the observed PS and PDF.

The RSI model matches the PS somewhat better than our fiducial scale-invariant model ($\sigma_8 = 0.9$), but overestimates the PDF in the range $F \gtrsim 0.6$ unless the temperature is very high, $\hat{T}_4 \gtrsim 2$. This conclusion holds provided that continuum fitting error and noise have a negligible impact on the PDF for $0.1 \gtrsim F \gtrsim 0.8$. A scale-invariant model with $\sigma_8 = 0.9$ matches better the flux PDF but tend to overestimate $\Delta_F^2(k)$ on scale $k \lesssim 0.01 \text{s km}^{-1}$ at large temperature $\hat{T}_4 \gtrsim 1.5$. Therefore, at fixed temperature $\hat{T}_4 \gtrsim 1.5$, the agreement with the measured $\Delta_F^2(k)$ is better for lower σ_8 . Models which match best the PS data alone do not yield a good fit of the PDF. The discrepancy worsens with decreasing temperature. In the fiducial scale-invariant cosmology, the disagreement in the PDF is really severe for $\hat{T}_4 \gtrsim 2$. Including the PDF in the fit increases $\Delta_F^2(k)$ on scale $k \lesssim 0.01 \text{s km}^{-1}$ by about 10%. It is therefore important to combine the PS and PDF in order to ensure that both statistics are correctly reproduced. Otherwise, the constraints inferred from $\Delta_F^2(k)$ alone might be significantly biased. Furthermore, a joint fit of the flux PS and PDF can help distinguishing between models with similar σ_8 , but different spectral index (cf. Fig 7). We computed the line statistics for a few best fit models. All of them successfully reproduce the slope and normalisation of the column density distribution $f(N_{\text{HI}})$, as well as the overall line width distribution $f(b)$. The line statistics thus do not offer additional constraints on the shape and normalisation of the primordial power spectrum when the model parameters assume their best fit values. We have not explored the sensitivity of our results to the mean flux level $\langle F \rangle$ since this issue has already been extensively investigated (e.g. Seljak, McDonald & Makarov 2003; Viel, Haehnelt & Springel 2004). The prior $\langle F \rangle \gtrsim 0.684 \pm 0.023$ (M00) is nevertheless consistent with other high-resolution observations of the Ly α forest (e.g. Kim *et al.* 2004; see however McDonald *et al.* 2004b who adopt a slightly lower value and larger errorbars).

Degeneracies among the parameters diminish the ability of the data to constrain the shape and normalisation

of the primordial power spectrum (e.g. Zaldarriaga, Hui & Tegmark 2001; Zaldarriaga, Scoccimarro & Hui 2003). For example, the parameters γ and k_F , as well as \hat{T}_g and σ_8 , are degenerated at constant mean flux. To make progress, we assumed that the filtering scale $1/k_F$ is related to the IGM temperature according to $k_F \propto \hat{T}_g^{-1/2}$. We briefly discuss the reasons motivating this choice in Appendix §A. In Table 3, we list the best fit parameter values for a fixed $\gamma = 1.3$, consistent with observations at $z = 3$ (e.g. Schaye *et al.* 2000). We believe that a value $k_F(\hat{T}_4 = 1) = 8$ provides a reliable upper limit on the filtering length $1/k_F$ (see Appendix A). This implies $\sigma_8 \lesssim 0.9$. Furthermore, for a large filtering $k_F(1) > 10 \text{ } h\text{Mpc}^{-1}$, the best fit value of σ_8 is larger than $\sigma_8 \gtrsim 0.65$, even for a temperature as high as $\hat{T}_4 \gtrsim 2$. Therefore, we expect $\sigma_8 = 0.8 \pm 0.1$ for a temperature $1 \lesssim \hat{T}_4 \lesssim 2$ and a reasonable reionization scenario. Note however that, at temperature $\hat{T}_4 \gtrsim 1.5$, a model with $\sigma_8 \lesssim 0.8$ matches the data better than a model with $\sigma_8 \gtrsim 0.8$, which tends to overestimate $\Delta_F^2(k)$ in the range $k \lesssim 0.01 \text{s km}^{-1}$ (cf. Section 4.3). Systematic errors in the modeling of the Ly α forest are expected to be large (e.g. Viel, Haehnelt & Springel 2004), making difficult to infer tight constraints for σ_8 . In particular, it is difficult to constrain the filtering k_F as a result of uncertainties in the relation between baryons and dark matter, and in the reionization history (e.g. Zaldarriaga, Hui & Tegmark 2001). Our findings are however consistent with other analysis of the Ly α forest which favour a scale-invariant cosmology with $\sigma_8 = 0.85 - 0.95$ (e.g. Viel, Haehnelt & Springel 2004; McDonald *et al.* 2004). In particular, our results show that it is difficult to tightly constrain the shape and normalisation of the linear power spectrum from the Ly α flux without combining several statistics of the Ly α forest. In this respect, the bispectrum offers an interesting alternative to the PDF (Mandelbaum *et al.* 2003), since it should be less sensitive than the PDF to systematic errors such as continuum fitting.

6 ACKNOWLEDGEMENT

We thank Martin Haehnelt, Michael Rauch, Ravi Sheth, David Tytler, and Matteo Viel for stimulating discussions. This Research was supported by the German Israeli Foundation for Scientific Research and Development, the EC RTN network “The Physics of the Intergalactic Medium”, and the United States-Israel Bi-national Science Foundation. We would like to acknowledge the Institute of Astronomy (Cambridge) and The University of Pittsburgh where part of this work was accomplished.

REFERENCES

- Bahcall J.N., Salpeter E.E., 1965, ApJ, 142, 1677
- Bennett C.L. *et al.* , 2003, ApJS, 148, 1
- Bi H.G., 1993, ApJ, 405, 479
- Bi H.G., Börner G., Chu Y., 1992, A&A, 266, 1
- Bi H.G., Davidsen A.F., 1997, ApJ, 479, 523
- Bryan G.L., Machacek M., Anninos P., Norman M.L., 1999, ApJ, 517, 13

Burles S., Tytler D., 1998, ApJ, 499, 699

Carswell R.F., Webb J.K., Cooke A.J., Irwin M.J., 2003, Voigt Profile Fitting Program Version 5. Available on-line at <http://www.ast.cam.ac.uk/rpc/vpfit.html>

Cen R., Miralda-Escudé J., Ostriker J.P., Rauch M., 1994, ApJ, 437, L83

Cen R., Ostriker J.P., 1999, ApJ, 519, L109

Coles P., Jones B., 1991, MNRAS, 248, 1

Croft R.A.C., Weinberg D.H., Katz N., Hernquist L., 1998, ApJ, 495, 44

Croft R.A.C., Weinberg D.H., Bolte M., Burles S., Hernquist L., Katz N., Kirkman D., Tytler D., 2002, ApJ, 581, 20

Croft R.A.C., 2004, ApJ, 610, 642

Davé R. *et al.*, 2001, ApJ, 552, 473

Desjacques V., Nusser A., Haehnelt M.G., Stoehr F., 2004 MNRAS, 350, 879

Eisenstein D.V., Hu W., 1999, ApJ, 511, 5

Gnedin N.Y., Hui L., 1998, MNRAS, 296, 44

Gnedin N.Y., Hamilton A.J.S., 2002, MNRAS, 334, 107

Gunn J.E., Peterson B.A., 1965, ApJ, 142, 1633

Hernquist L., Katz N., Weinberg D.H., Miralda-Escudé J., 1996, ApJ, 457, L51

Hu E.M., Kim T.-S., Lennox L.C., Songaila A., Rauch M., 1995, AJ, 110, 1526

Hui L., Gnedin N.Y., 1997, MNRAS, 292, 27

Hui L., Gnedin N.Y., Zhang Y., 1997, ApJ, 486, 599

Hui L., Burles S., Seljak U., Rutledge R.E., Magnier E., Tytler D., 2001, ApJ, 552, 15

Katz N., Weinberg D.H., Hernquist L., 1996, ApJS, 105, 19

Kim T.-S., Hu E.M., Cowie L.L., Songaila A., 1997, AJ, 114, 1

Kim T.-S., Carswell R.F., Cristiani S., D'Odorico S., Giallongo E., 2002, MNRAS, 335, 555

Kim T.-S., Viel M., Haehnelt M.G., Carswell R.F., Cristiani S., 2004, 347, 335

Mandelbaum R., McDonald P., Seljak U., Cen R., 2003, MNRAS, 344, 776

Matarrese S., Mohayaee R., 2002, MNRAS, 329, 37

McDonald P., Miralda-Escudé J., Rauch M., Sargent W.L.W., Barlow T.A., Cen R., Ostriker J.P., 2000, ApJ, 543, 1

McDonald P., Miralda-Escudé J., Rauch M., Sargent W.L.W., Barlow T.A., Cen R., 2001, ApJ, 562, 52

McDonald P., Miralda-Escudé J., 2001, ApJ, 549, L11

McDonald P., 2003, ApJ, 585, 34

McDonald P. *et al.*, 2004a, ArXiv Astrophysics e-prints, astro-ph/0405013

McDonald P. *et al.*, 2004b, ArXiv Astrophysics e-prints, astro-ph/0407377

McDonald P., Seljak U., Cen R., Bode P., Ostriker J.P., 2004c, ArXiv Astrophysics e-prints, astro-ph/0407378

McGill C., 1990, MNRAS, 242, 544

Miralda-Escudé J., Cen R., Ostriker J.P., Rauch M., 1996, ApJ, 471, 582

Nath B.B., Silk J., 2001, MNRAS, 327, 5

Nusser A., Haehnelt M.G., 2000, MNRAS, 313, 364

Nusser A., 2000, MNRAS, 317, 902

Peebles P.J.E., 1984, ApJ, 277, 470

Petitjean P., Webb J.K., Rauch M., Carswell R.F., Lanzetta K., 1993, MNRAS, 262, 499

Petitjean P., Mücket J.P., Kates R.E., 1995, A&A, 295, L9

Rauch M. *et al.*, 1997, ApJ, 489, 7

Rauch M., 1998, ARA&A, 36, 267

Reisenegger A., Miralda-Escudé J., 1995, ApJ, 449, 476

Ricotti M., Gnedin N.Y., Shull J.M., 2000, ApJ, 534, 41

Schaye J., Theuns T., Rauch M., Efstathiou G., Sargent W.L.W., 2000, MNRAS, 318, 817

Seljak U., McDonald P., Makarov A., 2003, MNRAS, 342, L79

Spergel D.N. *et al.*, 2003, ApJS, 148, 175

Springel V., Yoshida N., White S.D.M., 2001, New Astronomy, 6, 79

Tegmark M., Zaldarriaga M., 2000, ApJ, 544, 30

Theuns T., Leonard A., Efstathiou G., Pearce F.R., Thomas P.A., 1998, MNRAS, 301, 478

Viel M., Matarrese S., Heavens A., Haehnelt M.G., Kim T.-S., Springel V., Hernquist L., 2004a, MNRAS, 347, L26

Viel M., Haehnelt M.G., Carswell R.F., Kim T.-S., 2004b, MNRAS, 349, L33

Viel M., Haehnelt M.G., Springel V., 2004, submitted to MNRAS, astro-ph/0404600

Viel M., Weller J., Haehnelt M.G., 2004, submitted to MNRAS, astro-ph/0407294

Zaldarriaga M., Hui L., Tegmark M., 2001, ApJ, 557, 519

Zaldarriaga M., Scoccimarro R., Hui L., 2003, ApJ, 590, 1

Zhang Y., Anninos P., Norman M.L., 1995, ApJ, 453, L57

APPENDIX A: THE FILTERING LENGTH

Gas pressure smoothes the gas distribution relative to that of the dark matter. This effect becomes important below a (comoving) scale $1/k_J$, the Jeans scale, which is defined as (e.g. Bi, Börner & Chu 1992)

$$\frac{1}{k_J} = \frac{1}{aH} \sqrt{\frac{2\gamma k_B \hat{T}_g}{3\mu}} = 0.176 h^{-1} \text{Mpc} \left(\frac{\gamma \hat{T}_4}{1+z} \right)^{1/2}, \quad (\text{A1})$$

where a is the scale factor, H the Hubble constant, k_B the Boltzmann constant and μ the mean molecular weight. Here, γ describes the temperature-density relation, $T_g = \hat{T}_g(1 + \delta_g)^{\gamma-1}$. The numerical estimate was obtained for a Λ CDM cosmology with matter content $\Omega_m = 0.3$, assuming $\mu = 0.59$, a value appropriate for a fully ionized plasma of primordial abundance. The filtering scale $1/k_F$ over which the gas is smoothed will generally differ from the Jeans scale $1/k_J$. The redshift evolution of k_F is complex, and depends on the details of the reionization scenario, i.e. on the whole time evolution of k_J . However, for some particular choices of reionization history (e.g. sudden reionization), it is possible to work out analytic solutions to the *linear* equation governing the evolution of baryonic and dark matter in a EdS Universe (e.g. Peebles 1984; Bi, Börner & Chu 1992; Gnedin & Hui 1998; Nusser 2000; Matarrese & Mohayaee 2002). Under these assumptions, Gnedin & Hui (1998) pointed out that, at redshift $z = 3$, $k_F = \eta k_J$ with $\eta \sim 1.5 - 2.5$ for realistic reionization scenarios. Taking $\gamma = 1.3$ and $\hat{T}_4 = 1.5$, we have $k_F \approx 5.8\eta h \text{Mpc}^{-1}$. Note that we divided k_F by $\sqrt{2}$ to account for our definition of the filter, which reduces to $W \simeq 1 - k^2/2k_F^2$ on large scale. Note that, for a scale-invariant cosmology with $\sigma_8 = 0.9$, this theoretical prediction is substantially larger than the best fit values $k_F = 6 - 9 h \text{Mpc}^{-1}$ (cf. Section §4) unless η is significantly low, $\eta \lesssim 1.5$ (i.e. reionization happened at relatively high redshift).

In this paper, we smooth the Fourier modes of the dark matter density field with a uniform Gaussian filter $W = \exp(-k^2/2k_F^2)$ to obtain the gas density and velocity fields. In reality, we expect the filtering length $x_F(\mathbf{x}, t)$ to be a function of space and time through the local temperature and density. To get an idea of this dependence, we

consider a spherical perturbation. The gravitational acceleration, mainly due to dark matter, at a physical distance $r = x_F/(1+z)$ from the perturbation center is $GM/r^2 \propto r\rho_m^{\text{th}}$, where ρ_m^{th} is the dark matter density smoothed with a top-hat window of comoving width x_F . By equating this gravity term to the pressure term $[\text{d}P(r)/\text{d}r]/\rho_g(r)$, we express x_F as

$$x_F = \sqrt{\frac{\pi c_S^2}{G\rho_m^{\text{th}}}}(1+z), \quad (\text{A2})$$

where $c_S = (\text{d}P/\text{d}\rho_g)^{1/2}$ is the local speed of sound. The density ρ_m^{th} is not equal to the gas density. However, both are tightly related and have similar dependence on x_F . Hence, if we assume that $\rho_m^{\text{th}} \propto \rho_g$, and that the gas temperature and density follow the powerlaw relation mentioned above, we have

$$x_F(z, \delta_g) = \hat{x}_F(z)(1+\delta_g)^{\gamma/2-1}, \quad (\text{A3})$$

where $\hat{x}_F(z)$ is the filtering length at mean density. For an adiabatic index $1 \lesssim \gamma \lesssim 1.6$, eq. (A3) implies that x_F depends only weakly on δ_g . However, a uniform smoothing scale will tend to overestimate (underestimate) the gas density in the low (high) density regions. Therefore, we also expect a non-uniform smoothing $x_F(z, \delta_g)$ to affect the value of k_F , which is obtained in the limit of small wavenumbers.

To assess the importance of this effect, we assume that the gas density can be obtained locally from the dark matter density as follows :

$$1 + \delta_g(\mathbf{x}) = \int \frac{d^3y}{(2\pi)^{3/2}x_F^3} [1 + \delta_m(\mathbf{y})] e^{-\frac{(\mathbf{x}-\mathbf{y})^2}{2x_F^2}}. \quad (\text{A4})$$

In principle, the filtering length $x_F = x_F(\delta_g)$ should depend on the local gas density, and eq. (A4) would implicitly define δ_g . For simplification however, we will assume that $x_F = x_F(\delta_m) = \hat{x}_F(1+\delta_m)^{\gamma/2-1}$ (cf. equation A3). The Fourier transform of the gas density field is simply given by

$$\delta_g(\mathbf{k}) + \delta_D(\mathbf{k}) = \int \frac{d^3x}{(2\pi)^3} [1 + \delta_m(\mathbf{x})] e^{-\frac{1}{2}k^2x_F^2} e^{-i\mathbf{k}\cdot\mathbf{x}}, \quad (\text{A5})$$

where $\delta_D(\mathbf{k})$ is the Dirac delta function. The gas power spectrum is then (ignoring the term at $\mathbf{k} = 0$)

$$P_g(\mathbf{k}) = \int \frac{d^3r}{(2\pi)^3} \langle (1 + \delta_m)(1 + \delta'_m) e^{-\frac{1}{2}k^2(x_F^2+x'_F^2)} \rangle e^{-i\mathbf{k}\cdot\mathbf{r}}, \quad (\text{A6})$$

where the fields δ_m , x_F and δ'_m , x'_F are evaluated at position \mathbf{x} and $\mathbf{x} + \mathbf{r}$ respectively. $P_g(\mathbf{k})$ is thus the Fourier transform of a mass-weighted filter,

$$\mathcal{Z}_g[k, \mathbf{r}] = \langle (1 + \delta_m)(1 + \delta'_m) e^{-\frac{1}{2}k^2(x_F^2+x'_F^2)} \rangle. \quad (\text{A7})$$

To estimate k_F , we consider the limit of small wavenumbers $k \rightarrow 0$. Since the integrand is weighted by r^2 , we expect the main contribution to the integral to arise in the limit $|\mathbf{r}| \rightarrow \infty$. Expand the previous equation to first order in k

and taking the limit $|\mathbf{r}| \rightarrow \infty$, we have

$$\begin{aligned} \mathcal{Z}_g[k, \mathbf{r}] &\approx (1 + \xi_m(r)) - \frac{k^2}{2} \langle (1 + \delta_m)(1 + \delta'_m)(x_F^2 + x'_F^2) \rangle \\ &= (1 + \xi_m(r)) \left[1 - k^2 \frac{\langle (1 + \delta_m)(1 + \delta'_m)x_F^2 \rangle}{1 + \xi_m(r)} \right] \\ &\approx (1 + \xi_m(r)) \left[1 - k^2 \langle (1 + \delta_m)x_F^2 \rangle \right]. \end{aligned} \quad (\text{A8})$$

Hence, in the limit $k \rightarrow 0$, the gas power spectrum can be expressed as

$$P_g(\mathbf{k}) \simeq \left(1 - \frac{k^2}{k_F^2} \right) P_m(\mathbf{k}), \quad (\text{A9})$$

where k_F is an effective filtering length defined as

$$\frac{1}{k_F^2} = \langle (1 + \delta_m)x_F^2 \rangle = \frac{1}{\hat{k}_F^2} \int d\delta_m \mathcal{P}(\delta_m) (1 + \delta_m)^{\gamma-1}, \quad (\text{A10})$$

which differ from the filtering length $\hat{k}_F = 1/\hat{x}_F$ at mean density. Here, $\mathcal{P}(\delta_m)$ is the one-point probability distribution of the dark matter density field. Eq. (A10) shows that, in the linear regime, k_F is obtained from a mass-weighted average of the local filtering length x_F . To evaluate k_F , we will assume that the dark matter PDF is well approximated by a lognormal distribution,

$$\mathcal{P}(\delta_m)d\delta_m = \frac{1}{\sqrt{2\pi}\sigma_L} e^{-\nu^2/2\sigma_L^2} d\nu, \quad (\text{A11})$$

with $\nu = \ln(1 + \delta_m) + \sigma_L^2/2$, and where σ_L is the linear rms of dark matter fluctuations (Coles & Jones 1991). Although this approximation is inaccurate when $\sigma_L \gtrsim 1$, it should be sufficient to our purpose. A simple calculation yields

$$k_F^2 = \hat{k}_F^2 (1 + \sigma_{NL}^2)^{(\gamma-1)(2-\gamma)/2}, \quad (\text{A12})$$

where we have used $1 + \sigma_{NL}^2 = \exp(\sigma_L^2)$. k_F is larger than the filtering scale \hat{k}_F , but is a rather weak function of σ_{NL} . Furthermore, since x_F depends on the local gas density, we expect σ_{NL} to be a smoothed version of the dark matter rms fluctuation amplitude. It is nevertheless difficult to constrain the amplitude of this effect since the filtering length is not well constrained. However, since k_F is *always* larger than \hat{k}_F , we have certainly $k_F \gtrsim 6\eta h\text{Mpc}^{-1}$ for $\gamma = 1.3$ and $\hat{T}_4 = 1.5$. Therefore, we believe that $k_F(1) = 8 h\text{Mpc}^{-1}$ ($k_F(1) \equiv k_F(\hat{T}_4 = 1)$) is a reliable upper limit on the filtering scale at $z = 3$ for reasonable reionization histories of the Universe.